

## Research Paper

# Engineering temperature-sensitive plateletsomes as a tailored chemotherapy platform in combination with HIFU ablation for cancer treatment

Dongqi Wu, Xing Jin, Xiaobing Wang, Boyu Ma, Chenmei Lou, Haijing Qu, Jian Zheng, Binxuan Zhang, Xiufeng Yan, Yang Wang, Lijia Jing✉

Center for Bioactive Products, Northeast Forestry University/ Key Laboratory of Saline-Alkali Vegetation Ecology Restoration, Ministry of Education, Harbin 150040, China.

✉ Corresponding author: Lijia Jing, Tel/Fax: 86-451-82191230; Email: jinglijia@nefu.edu.cn

© Ivyspring International Publisher. This is an open access article distributed under the terms of the Creative Commons Attribution (CC BY-NC) license (<https://creativecommons.org/licenses/by-nc/4.0/>). See <http://ivyspring.com/terms> for full terms and conditions.

Received: 2018.12.11; Accepted: 2019.03.25; Published: 2019.05.31

## Abstract

Chemotherapy is widely used in combination with high-intensity focused ultrasound (HIFU) ablation for cancer therapy; however, the spatial and temporal integration of chemotherapy and HIFU ablation remains a challenge. Here, temperature-sensitive plateletsomes (TSPs) composed of platelet (PLT) membrane, 1-stearoyl-2-hydroxy-sn-glycero-3-phosphocholine and 1,2-dipalmitoyl-sn-glycero-3-phosphocholine were developed to adequately integrate chemotherapy with HIFU tumor ablation *in vivo*.

**Methods:** The thermosensitive permeability of TSPs was evaluated under both water bath heating and HIFU hyperthermia. The targeting performance, pharmacokinetic behavior and therapeutic potential of TSPs in combination with HIFU ablation were evaluated using HeLa cells and a HeLa cell tumor-bearing nude mouse model in comparison with temperature-sensitive liposomes (TSLs).

**Results:** TSPs showed high drug loading efficiency and temperature-sensitive permeability. When applied *in vivo*, TSPs showed a circulation lifetime comparable to that of TSLs and exhibited PLT-specific cancer cell affinity and a vascular damage response. Upon HIFU hyperthermia, TSPs displayed ultrafast drug release and enhanced tumor uptake, providing high drug availability in the tumor site to cooperate with HIFU ablation. After HIFU ablation, TSPs rapidly targeted the postoperative tumor site by adhesion to the damaged tumor vasculature, leading to targeted and localized postoperative chemotherapy.

**Conclusion:** Due to effective integration at both intraoperative and postoperative stages, TSPs could be a promising chemotherapy nanoplatform in combination with HIFU ablation for cancer therapy.

## Introduction

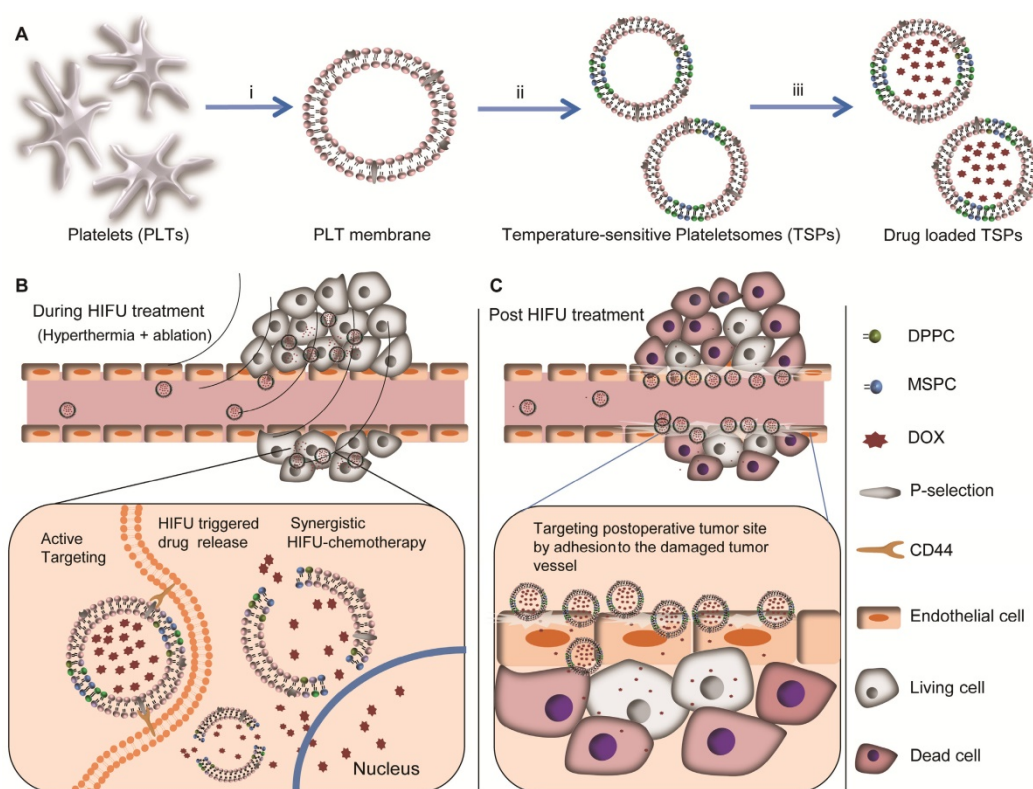
High-intensity focused ultrasound (HIFU) surgery, which employs focused ultrasound to ablate target lesions through a combined thermal-mechanical effect, has become a powerful therapeutic methodology for cancer [1-3]. Compared with surgery and radiotherapy, HIFU is a minimally invasive procedure [4,5]. Nevertheless, under a tolerated intensity, it is challenging for HIFU to completely eradicate a tumor because of the energy attenuation in deep-seated lesions [6-8]. To improve the outcome, the coadministration of HIFU and

chemotherapy is an important strategy [9,10]; however, the systemic administration of chemotherapeutic drugs often causes low therapeutic efficiency and severe side effects due to a lack of tumor selectivity.

For effective collaboration, ideal chemotherapies should target the tumor site before and after HIFU ablation and achieve efficient synergy at both intraoperative and postoperative stages. To achieve this goal, nanosized drug delivery systems (NDDSs) have been explored [11-13]. However, the

development of NDDSs with the abovementioned chemotherapeutic performance remains challenging. Among the existing NDDSs, poly(ethylene glycol) (PEG) modified temperature-sensitive liposomes (TSLs) have shown advantages in combination with HIFU tumor ablation due to the applicable circulation time and local hyperthermia-triggered ultrafast drug release by which enhanced drug availability was achieved in the tumor site [12,13]. However, the PEG corona hindered the tumor penetration and cancer cell uptake of liposomal drugs to some extent [14,15]. Postoperative chemotherapy is a critical step post HIFU ablation that can consolidate the therapeutic outcome and inhibit tumor recurrence. However, current TSLs are only used for HIFU-triggered intraoperative chemotherapy, and these molecules cannot adequately treat the postoperative residual tumor because HIFU ablation often causes vasculature damage and occlusion [16,17], which may inhibit the delivery of chemotherapy drugs to residual tumor tissues. Therefore, to achieve excellent synergistic HIFU chemotherapy, new types of TSLs that can address biological barriers to target the tumor site and effectively integrate chemotherapy with HIFU ablation in different treatment stages are highly desired.

Currently, endowing nanomedicines with biomimetic characteristics is a significant methodology to remarkably improve their therapeutic performance. Platelets (PLTs) are an important functional component of blood. Recent studies have demonstrated that antibodies and nanoparticles can be endowed with a long circulation lifetime, cancer cell adhesion and the vascular damage response by using PLTs as carriers or by using a PLT membrane (PM) coating strategy [18–28]. These PLT-mimicking platforms are promising for tumor therapy, especially for tumor target drug delivery [24–28]. In this study, to effectively integrate chemotherapy with HIFU tumor ablation, we fabricated PLT-mimicking TSLs named temperature-sensitive plateletsomes (TSPs) by employing PM and TSL-forming lipids of 1-stearoyl-2-hydroxy-sn-glycero-3-phosphocholine (MSPC) and 1,2-dipalmitoyl-sn-glycero-3-phosphocholine (DPPC) (Scheme 1A). Compared with previously reported PLT-mimicking NDDSs, TSPs showed not only PLT-mimicking properties but also thermal-triggered drug permeability. When administered systemically, TSPs provide efficient intraoperative chemotherapy with HIFU ablation by tumor targeting and HIFU-hyperthermia-triggered drug release (Scheme 1B), subsequently implementing



**Scheme 1.** Schematic design of temperature-sensitive plateletsomes (TSPs) as a tailored chemotherapy platform in combination with HIFU tumor ablation. (A) Main preparation process of drug-loaded TSPs: i) extraction of the PM from isolated PLTs; ii) preparation of TSPs by fusing the PM with MSPC and DPPC, followed by extruding the fused PM through 100-nm pores; iii) loading of doxorubicin (DOX) into TSPs. (B) DOX-loaded TSPs (DTSPs) could target cancer cells via the specific affinity between P-selectin and CD44 receptors, rapidly release the drug under HIFU hyperthermia, and implement highly efficient chemotherapy in combination with HIFU tumor ablation. (C) DTSPs can efficiently target postoperative tumor sites driven by HIFU-induced vascular damage and inflammation to implement ideal consolidation chemotherapy.

ideal postoperative chemotherapy by selective adhesion to the postoperative tumor sites driven by HIFU-induced tumor vascular damage and inflammation (Scheme 1C). Therefore, TSPs might serve as a tailored chemotherapy platform in combination with HIFU ablation for cancer therapy.

## Materials and methods

### Materials

PM was extracted from mouse PLTs according to our previous method [27]. DPPC, MSPC, 1-palmitoyl-2-(dipyrrometheneborondifluoride)undecanoyl-sn-glycero-3-phosphoethanolamine (TopFluor®PC, 495 nm/503 nm), 1-(dipyrrometheneboron difluoride)undecanoyl-2-hydroxy-sn-glycero-3-phosphocholine (TopFluor® Lyso PC) and 1,2-distearoyl-sn-glycero-3-phosphoethanolamine-N-[methoxy(polyethylene glycol)-2000] (DSPE-PEG<sub>2000</sub>) were obtained from Avanti Polar Lipids Inc. 1,1'-dioctadecyl-3,3',3'-tetramethylindotricarbocyanine (DiR) iodide (748 nm/780 nm) was purchased from AAT Bioquest Inc. Doxorubicin, Protease inhibitor cocktail (P8340) and methylthiazolyldiphenyltetrazolium bromide (MTT) were purchased from Sigma-Aldrich. Deionized water (18.2 MΩ cm) from a Milli-Q purification system was used in all preparations.

### Fabrication of nanoformulations

To synthesize TSPs, PM, DPPC and MSPC were added to phosphate-buffered saline (PBS, pH 7.4) containing a protease inhibitor cocktail. The mixture was incubated at 37 °C for 20 min and then homogenized by ultrasonication for 60 s at 100 W, followed by further incubation at 37 °C for 30 min. Finally, the mixture was extruded through 100-nm pores to obtain TSPs. To prepare TSLs, DPPC, MSPC and DSPE-PEG<sub>2000</sub> were dissolved in chloroform at a molar ratio of 86.5:9.7:3.8 in a round-bottom flask. After evaporation of the organic solvent, the resultant lipid film was vacuum-dried and hydrated in PBS at 37 °C. Then, the mixture was ultrasonicated for 60 s at 100 W. Finally, the mixture was extruded through 100-nm pores to obtain TSLs. Liposomes generated from DPPC and MSPC (named DMLs) were prepared by the same method used for fabricating TSLs by fixing the molar ratio of DPPC: MSPC to 80:20.

### Characterization of nanovesicles

The vesicle morphology was observed by transmission electron microscopy (TEM). The size distributions and zeta potentials of the vesicles were evaluated using a 90Plus/BI-MAS instrument (Brookhaven Instruments Co., USA). The phase transition temperature ( $T_m$ ) was examined using a

NETZSCH STA 449 F3 Jupiter® instrument. UV/Vis absorption spectra were measured using a Varian 4000 UV-Vis spectrophotometer. Western blotting was used to show the functional conservation of PLT biomarkers according to our previous method [27]. Proteins were extracted from PLT and TSPs. Protein solutions (not at the same concentration) were separated using SDS-PAGE electrophoresis and transferred onto polyvinylidene difluoride (PVDF) membranes. After a blocking step with 5% skim milk, the membrane was incubated with the primary antibody at 4 °C followed by incubation with the secondary antibody at room temperature. The bands were visualized using an enhanced chemiluminescence (ECL) plus detection system (GE Healthcare). To verify the right-side-out membrane orientation of the PM in TSPs, we incubated TSPs with FITC-labeled antibodies against P-selection and CD47. Subsequently, the incubated TSPs were purified through a sepharose column, and their fluorescence intensities were detected. For the control, DMLs were also evaluated.

### Drug loading and release

For all nanovesicles, a pH gradient method was used to encapsulate doxorubicin (DOX). Briefly, freshly prepared liposomal vesicles were sealed and dialyzed in citric acid buffer (pH 4.0) at 4 °C for 3 h. Then, the citrate buffer was rapidly exchanged with 20 mM HEPES buffer (pH 7.4) through a sepharose column. The suspension of vesicles (1 mg/mL) was then mixed with DOX (at a drug/vesicle weight ratio of 1:10), followed by incubation at 37 °C for 90 min. Then, free DOX was removed through a cation-exchange resin column. The encapsulation efficiency of DOX was determined by measuring the absorbance at 490 nm.

To evaluate the stability of DOX-loaded TSPs (DTSPs) in a biological environment, we investigated the drug leakage of DTSPs at 37 °C in RPMI-1640 medium containing 10% fetal bovine serum (FBS). The analysis was implemented according to our previous method for drug release monitoring [27]. The thermosensitive drug release was evaluated under both water bath heating and HIFU hyperthermia according to a previously reported method [34]. To investigate the drug release under water bath heating, 1 mL of DOX-loaded vesicles was added to a tube containing 20 mL of PBS with a stationary temperature in a water bath. At certain time intervals, 2 mL of the samples were taken from the tube and cooled by an ice-water mixture to quickly stop the drug release. To investigate HIFU hyperthermia-triggered drug release, 1 mL of DOX-loaded vesicles was added to a tube containing

20 mL of PBS at a stationary temperature under HIFU irradiation. At certain time intervals, 2 mL of samples were taken from the tube and cooled by an ice-water mixture to quickly stop the drug release. Cumulative drug release (%) was calculated by the following equation: cumulative drug release (%) =  $(F_t - F_0) / (F_c - F_0) \times 100\%$ .  $F_t$  is the fluorescence intensity of the sample treated by water bath heating or HIFU followed by cooling with an ice-water mixture.  $F_0$  is the fluorescence intensity of the sample with no treatment.  $F_c$  is the fluorescence intensity of DOX-loaded vesicles after being destroyed. The excitation and emission wavelengths for the fluorescence detection of DOX were 480 and 580 nm, respectively.

### Cell and tumor model

HeLa cells expressing a high level of CD44 were cultured at 37 °C and 5% CO<sub>2</sub>. RPMI-1640 medium containing 10% FBS, penicillin (100 U/mL), and streptomycin (100 mg/mL) was used as the culture medium. BALB/c nude mice were used for *in vivo* experiments. To establish the tumor model, 100 µL of PBS containing 5×10<sup>6</sup> HeLa cells was subcutaneously injected into the back of each mouse.

### Cellular uptake

To investigate cellular uptake, HeLa cells were incubated with TopFluor® PC-incorporated vesicles for different time points. The incubated cells were fixed with 4% formalin, treated with 10% Triton X-100 (TX-100) and stained with DAPI. Then, the cellular uptake of fluorescent vesicles was observed using confocal laser scanning microscopy. To quantify the cellular uptake of fluorescent vesicles, 2×10<sup>6</sup> cells were counted, and the fluorescence intensity of the cells was evaluated by flow cytometry.

### In vitro cytotoxicity

To investigate the potential of DOX-loaded TSPs-3 and TSLs (named DTSPs-3 and DTSLs, respectively) for routine chemotherapy, DTSPs-3 and DTSLs were incubated with HeLa cells for 24 h and 48 h. To investigate the potential of DTSPs-3 and DTSLs in HIFU hyperthermia-triggered chemotherapy, DTSPs-3 and DTSLs were incubated with HeLa cells for 1 h and then transferred into homemade tubes and exposed to HIFU hyperthermia at 42 °C for 2 min. Then, the cells were cultured in 48-well plates. To investigate the therapeutic potential of DTSPs-3 and DTSLs in combination with HIFU treatment (hyperthermia + ablation), DTSPs-3 and DTSLs were incubated with HeLa cells for 1 h. Subsequently, the incubated HeLa cells were exposed to HIFU hyperthermia (42 °C for 2 min), followed by treatment with ablative HIFU, and then the cells were cultured

for 24 h at 37 °C. Cell viability was evaluated using a MTT assay.

### Tumor uptake and pharmacokinetic study

To investigate the tumor targeting efficiency and pharmacokinetic behavior of the vesicles, TopFluor® PC-labeled vesicles were injected into tumor-bearing mice through the tail vein. For the TSPs-3-treated group, the PM was obtained from and administered to the same mice, and the vesicles were freshly made just before the injection. At various time points, blood, tissues and tumor samples were collected. Whole body near-infrared (NIR) fluorescence imaging of tumor-bearing mice was performed by detecting the fluorescence intensity of TopFluor® PC on an IVIS Spectrum In Vivo Imaging System (PerkinElmer, USA). The DOX and TopFluor® PC contents were detected by high-performance liquid chromatography (HPLC) to assess blood retention and the biodistribution of DOX and vesicles. All animal procedures were in agreement with the institutional animal use and care committee and carried out ethically and humanely.

### In vivo tumor therapy

Mice bearing HeLa cell tumors (with a size of approximately 100 mm<sup>3</sup>) were divided into 5 groups (n=6) and administered saline, HIFU treatment, HIFU treatment + DOX, HIFU treatment + DTSLs, and HIFU treatment + DTSPs-3. The DOX dosage was 20 mg/kg. For the DTSPs-3-treated group, the PM was obtained from and administered to the same mice. Both of the vesicles were freshly made and loaded with drugs just before the injection. HIFU treatment consists of HIFU hyperthermia (42 °C for 20 min) and closely followed HIFU ablation (30 s). For synergetic HIFU chemotherapy, the tumors were immediately treated with the abovementioned HIFU treatment after drug injection. A thermometer probe (0.8 mm in diameter) was inserted into the tumor to dynamically record the temperature. The tumor volume was calculated according to the following equation: tumor volume = (tumor length) × (tumor width)<sup>2</sup>/2. Tumor length and width were measured by a high precision digital vernier caliper. All animal procedures were in agreement with the institutional animal use and care committee and carried out ethically and humanely.

### HIFU equipment

The HIFU system was composed of an ultrasound generator (0~200 W output power and 0.6-1.8 MHz frequency) and an acoustic lens transducer (64 mm effective diameter and 60 mm focal length). For investigations of HIFU hyperthermia-triggered drug release and *in vitro* therapeutic performance, an acoustic transducer was

placed at the bottom of a degassed water tank, and ultrasound beams were focused on the samples (containing drug-loaded vesicles or test cells incubated with drug-loaded vesicles), which were transferred to a homemade tube and submerged under degassed water (Figure S9A). HIFU hyperthermia (~42 °C) was implemented by continuous-wave ultrasound (0.88 MHz and 21-23 W). HIFU ablation was implemented by continuous-wave ultrasound (1.21 MHz and 99-102 W). To investigate *in vivo* therapy, the tumor region was submerged under degassed water, and ultrasound beams were focused on the center of the tumor tissue (Figure S9B). HIFU hyperthermia (~42 °C) was implemented by continuous-wave ultrasound (0.88 MHz and 18-20 W). HIFU ablation was implemented by continuous-wave ultrasound (1.21 MHz and 91-93 W).

### Hematology

Blood samples were collected from the mice ethically and humanely. The blood cell analysis was conducted on a fully automatic hematology analyzer (Hanfang Instruments Co., China). The blood biochemical index analysis was conducted on a semiautomatic biochemistry analyzer (Hanfang Instruments Co., China).

### Histological analysis

Tumors and major organs, including the liver, heart, kidneys, spleen and lungs, were collected ethically and humanely. For hematoxylin and eosin (H&E) staining, the tissue samples were fixed with 4% formalin and then embedded in paraffin before sectioning. For standard immunohistochemistry staining, the tissue samples were harvested and frozen in optimum cutting temperature (OCT) compound before sectioning. The immunohistochemistry and H&E samples were imaged with a microscope.

### Statistical analysis

Student's t-test was used to analyze the significance of the difference between the groups. One-way analysis of variance (ANOVA) was applied (\* $p < 0.05$ , \*\* $p < 0.01$ , and \*\*\* $p < 0.001$ ).

## Results and Discussion

### Fabrication and characterization of TSPs.

TSPs were fabricated by the following steps: (1) extraction of the PM from fresh PLTs, (2) fusion of DPPC and MSPC with the PM and (3) extrusion of the lipid-fused PM into nanovesicles. PLTs were isolated from fresh mouse blood (Figure S1) and subjected to a repeated freeze-thaw process to extract pelleted PM (Figure 1B1). To demonstrate that DPPC and MSPC

can fuse with the PM, TopFluor® PC and TopFluor® Lyso PC with green fluorescence were incubated with the DiR iodide-stained PM. As observed in Figure 1A, after incubation, the PM showed bright green fluorescence from the lipids, which merged well with the red fluorescence from DiR iodide, indicating the successful fusion of the PM with the lipids. TSPs were obtained by extruding the fused PM through 100 nm pores. To modulate the thermosensitive permeability of TSPs, the content of DPPC and MSPC in TSPs was set at 20, 35, 50 and 65 wt.% by fixing the molar ratio of DPPC:MSPC to 80:20. Here, TSPs containing 20, 35, 50 and 65 wt.% DPPC and MSPC are abbreviated as TSPs-1, TSPs-2, TSPs-3 and TSPs-4, respectively. Figure 1B shows that all TSPs were spherical and well dispersed under TEM, comparable to the nanovesicles made from pure PM (NPVs). By extrusion, all the nanovesicles could be adjusted to a similar size distribution (Table S1). Increasing amounts of DPPC and MSPC caused decreasing surface charge and PLT protein content in TSPs (Figure 1C). Nonquantitative western blot analysis demonstrated the functional conservation of PLT biomarkers, including CD36, CD42d, CD47 and P-selectin, on the TSPs (Figure 1D). CD36 and CD42d play important roles in blood vessel adhesion. P-selectin can mediate the specific binding of TSPs to the CD44 receptor on cancer cells [24]. CD47, an immunomodulatory protein, can inhibit the macrophage uptake of TSPs. By incubation with FITC-labeled antibodies against P-selectin and CD47, TSPs showed increased fluorescence intensity as the PM content increased, but DMLs showed nearly no fluorescence (Figure S2). This result demonstrated that the PM in TSPs has a right-side-out membrane orientation. The above results provide a solid foundation for the PLT-mimicking biological properties of TSPs. The  $T_m$  is an important parameter for indicating the temperature-sensitive properties of temperature-sensitive liposomal vesicles. In this study, we evaluated the  $T_m$  values of all TSPs by differential scanning calorimetry (DSC). The  $T_m$  values of TSPs-1, TSPs-2, TSPs-3 and TSPs-4 were 51.8, 46.32, 42.52 and 42.16 °C (Figure 2A), respectively, which were all lower than that of the pure PM ( $T_m$  value of 58.5 °C). This result demonstrated that the increased proportions of DPPC and MSPC decreased the  $T_m$  values of TSPs, making these particles more suitable for ultrafast drug release at low temperatures.

### Drug encapsulation and temperature-sensitive drug release from TSPs.

The temperature-sensitive drug release profiles of TSPs were investigated using DOX as a model drug. A pH gradient method was used to encapsulate

DOX into TSPs. At a drug/vesicle weight ratio of 1:10, all TSPs showed high drug encapsulation efficiencies over 80% (Table S1). The DOX-loaded TSPs (DTSPs) showed the characteristic absorption of DOX in the UV-vis-NIR spectrum (Figure 2B) and displayed the red fluorescence of DOX under microscopy (Figure S3). We evaluated the stability of DTSPs in a simulated biological environment (at 37 °C in RPMI-1640 medium containing 10% FBS). As shown in Figure S4, four DTSP formulations displayed a similar sustained release of DOX in the simulated environment, which would ensure good stability for *in vivo* tumor drug delivery. Next, we evaluated the drug release behavior of DTSPs in a water bath at temperatures ranging from 37 to 42 °C within 2 min. DOX loaded TSLs (DTSLs), which are composed of DPPC, MSPC and DSPE-PEG<sub>2000</sub>, were used for comparison [29]. As shown in Figure 2C, almost no drug was released from DTSLs and DTSPs at 37 °C over 2 min. With increasing temperature, DTSLs and DTSPs showed accelerated drug release at different levels. When heated to 42 °C, DTSLs released nearly 100% of the drug within 2 min, and the drug release rates of DTSPs-1, DTSPs-2, DTSPs-3 and DTSPs-4 reached 6.93%, 15.12%, 83.4% and 89.33%, respectively. In theory, 42 °C is the critical temperature to induce cancer cell apoptosis [30, 31].

Therefore, we expected that TSPs-3 and TSPs-4, which showed high temperature-sensitive permeability at 42 °C, could rapidly release drugs before HIFU ablation, thereby producing efficient chemotherapy in cooperation with HIFU ablation at the tumor site. Then, we investigated the drug release profiles of DTSPs-3 and DTSPs-4 under HIFU hyperthermia. The HIFU beam was focused on a solution containing drug-loaded vesicles. By adjusting the ultrasonic power and frequency, the solution temperature was maintained at ~42 °C. As shown in Figure 2D, under HIFU hyperthermia at 42 °C, the drug release from DTSPs-3 and DTSPs-4 reached approximately 100% within 2 min, which was comparable to that from DTSLs. By TEM observation (Figure 2E), we found that compared to water bath heating, HIFU treatment induced a perforation effect on TSPs. This result is attributed to the intrinsic thermomechanical effect of HIFU [32,33]. The cavitation effect during HIFU hyperthermia mechanically perforated TSPs, thus facilitating accelerated drug release. Compared with TSPs-4, TSPs-3 had a comparable HIFU-triggered drug release but a high PLT protein content. Therefore, we selected TSPs-3 for further investigations because a high PLT protein content is advantageous to impart TSPs with PLT-mimicking biological properties.

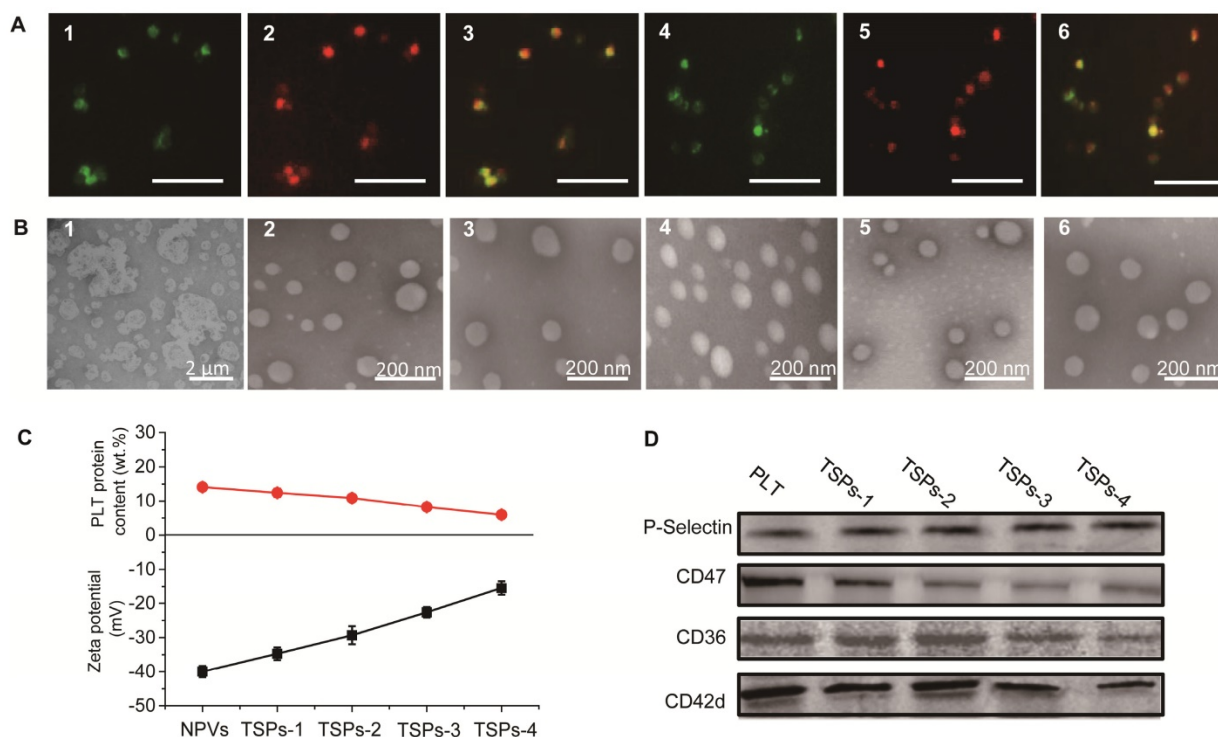


**Figure 1.** (A) Fluorescence microscopy images of a DiR iodide-stained PM incorporated with fluorescent lipids: 1) TopFluor® PC signal of a TopFluor® PC-incorporated PM, 2) DiR iodide signal of a TopFluor® PC-incorporated PM, 3) merged image of 1) and 2), 4) TopFluor® Lyso PC signal of a TopFluor® Lyso PC-incorporated PM, 5) DiR iodide signal of a TopFluor® Lyso PC-incorporated PM, and 6) merged image of 4) and 5). The scale bar represents 5  $\mu$ m. (B) TEM images of 1) PM, 2) NPVs, 3) TSPs-1, 4) TSPs-2, 5) TSPs-3 and 6) TSPs-4. (C) PLT protein content and zeta potentials of NPVs and different TSPs. (D) Identification of PLT and different TSPs for CD36, CD42d, CD47 and P-selectin biomarkers by western blot analysis.

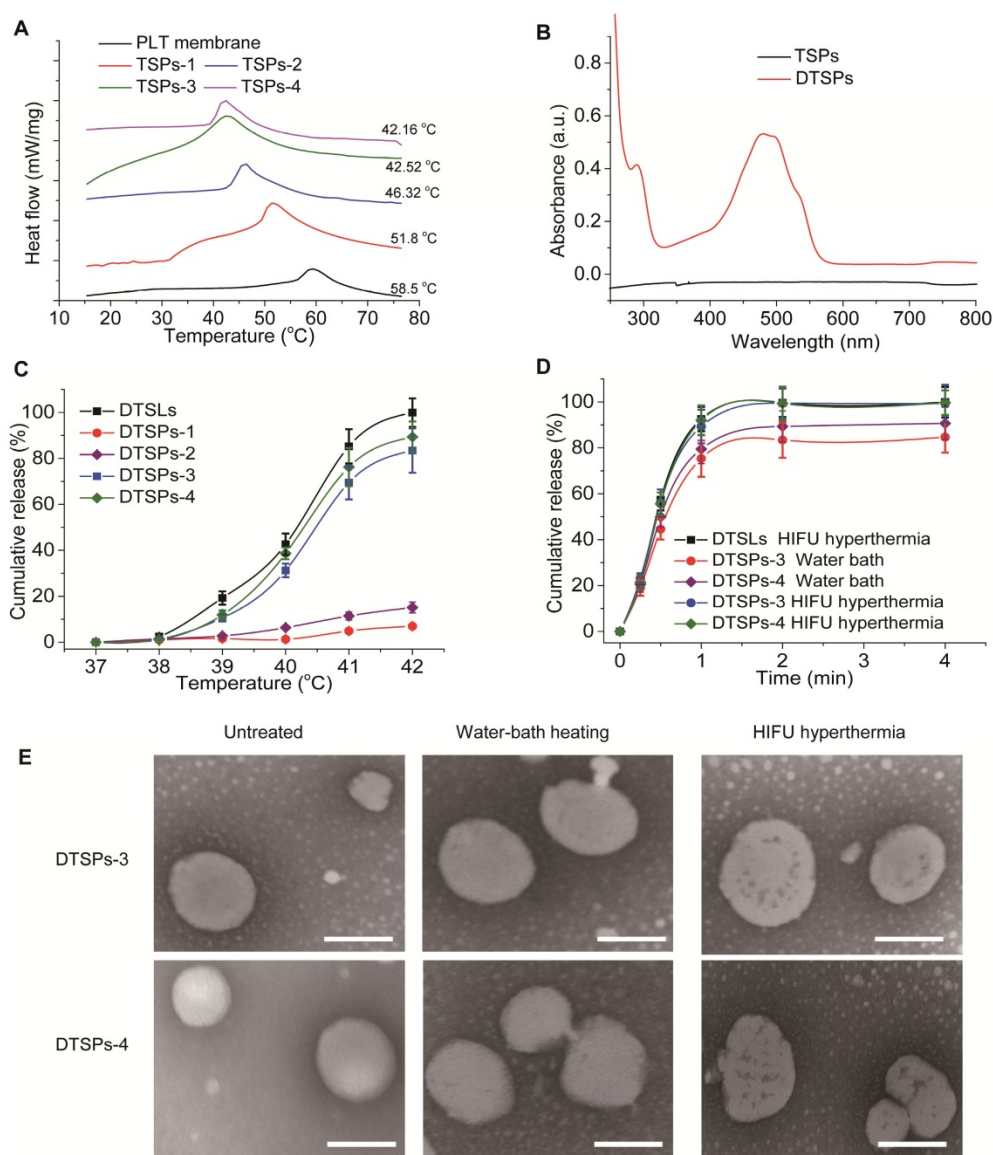


**Figure 2.** (A) DSC curves of the PM and different TSPs. (B) UV-vis spectra of the TSPs loaded with or without DOX. (C) Effect of the vesicular composition on the DOX release behavior of TSPs at different temperatures under water bath heating for 2 min. (D) Comparison of DOX release profiles from DTSPs-3 and DTSPs-4 at 42 °C under water bath heating or HIFU hyperthermia. (E) TEM images of DTSPs-3 and DTSPs-4 after no treatment, water bath heating (42 °C, 2 min) and HIFU hyperthermia (42 °C, 2 min). The scale bar represents 100 nm.

### **In vitro** evaluation of the cancer cell affinity of TSPs-3.

The cancer cell affinity of TSPs-3 was investigated *in vitro*. For comparison, TSLs and DMLs were investigated under the same conditions. All vesicles were incorporated with the same amount of TopFluor® PC; therefore, the cell-vesicle interactions could be visualized and quantified through a fluorescent signal. The cancer cell affinities of these vesicles were evaluated by monitoring their cellular uptake in HeLa cells overexpressing CD44. By observing and measuring the intracellular fluorescence intensity (Figure 3A,B), we found that TSLs, DMLs and TSPs-3 were internalized by HeLa cells in a time-dependent manner. Compared with

DMLs and TSPs-3, TSLs were less internalized by HeLa cells. This result is attributed to stable PEG coronas on TSLs, which can decrease the affinity of the vesicles for cancer cells, thereby suppressing the cellular uptake of the vesicles. Notably, significantly higher fluorescence intensity was observed in TSPs-3-incubated cells than in DML-incubated cells at different incubation times (2.1-fold higher at 1 h; 2.5-fold higher at 4 h; 1.9-fold higher at 8 h). We assumed that the preferential internalization of TSPs-3 by HeLa cells is attributed to the high affinity between P-selectin and CD44 receptors. To investigate this hypothesis, a P-selectin antibody was used to block the interaction between TSPs-3 and HeLa cells. The P-selectin antibody significantly diminished the intracellular uptake of TSPs-3 by HeLa cells (Figure

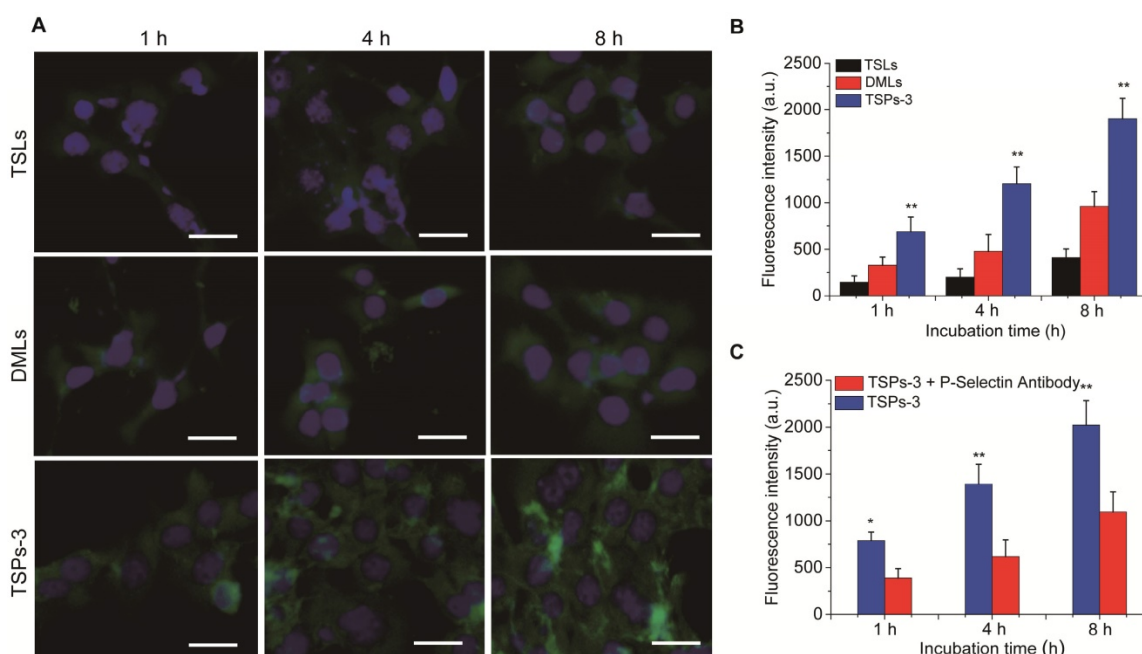


**Figure 3.** (A) Intracellular uptake of TopFluor® PC-doped TSLs, DMLs and TSPs-3 at a concentration of 50  $\mu\text{g}/\text{mL}$  in HeLa cells after 1, 4 and 8 h of incubation. The scale bar represents 20  $\mu\text{m}$ . (B) Fluorescence intensities of HeLa cells after incubation with TopFluor® PC-doped TSLs, DMLs and TSPs-3 at a concentration of 50  $\mu\text{g}/\text{mL}$  for 1, 4 and 8 h. (C) Comparison of the fluorescence intensities of HeLa cells after incubation with TopFluor® PC-doped TSPs-3 and TopFluor® PC-doped TSPs-3 + P-selectin antibody.

3C). This result provides strong evidence that P-selectin can significantly improve the targeting ability of TSPs-3 to HeLa cells. The active targeting ability of TSPs-3 is advantageous for the specific targeted delivery of drugs to tumor sites overexpressing CD44 receptors.

### **In vitro therapeutic performance of DTSPs-3.**

The potential of DTSPs-3 in routine chemotherapy, HIFU hyperthermia-triggered chemotherapy and combination therapy with HIFU ablation was investigated in HeLa cells. DTSLs were used for comparison. The biocompatibilities of TSPs-3 and TSLs were first evaluated. Both vesicles showed almost no toxicity to HeLa cells, even at a high incubating concentration (200  $\mu\text{g}/\text{mL}$ ) for 48 h, indicating the reliable biosafety of these particles (Figure S5). After routine incubation with HeLa cells, DTSPs-3 had IC<sub>50</sub> values of  $12.56 \pm 1.37 \mu\text{M}$  and  $7.89 \pm 0.92 \mu\text{M}$  against HeLa cells after 24 h and 48 h, respectively; these values were lower than those for DTSLs ( $28.21 \pm 1.98 \mu\text{M}$  after 24 h and  $18.46 \pm 0.79 \mu\text{M}$  after 48 h), indicating that the chemotherapeutic performance of DTSPs-3 is greater than that of DTSLs (Figure 4A). To investigate HIFU hyperthermia-triggered chemotherapy, HeLa cells were incubated with drug-loaded vesicles for 1 h, transferred to homemade tubes and exposed to HIFU hyperthermia at 42 °C for 2 min (Figure 4B). Thereafter, the incubated cells were further cultured in 48-well plates until the viability test. This hyperthermia treatment did not affect the viability of cancer cells (Figure S6)

but accelerated drug release from DTSPs-3 and DTSLs in target cells (Figure 4C). Both DTSPs-3 and DTSLs exhibited improved cytotoxicity against HeLa cells under HIFU hyperthermia. The IC<sub>50</sub> values of DTSPs-3 and DTSLs against HeLa cells at 24 h and 48 h were decreased by more than 50% compared with routine chemotherapy values (Figure 4D). Notably, DTSPs-3 always exhibited enhanced chemotherapeutic cytotoxicity to HeLa cells compared with DTSLs either with or without hyperthermia treatment, which is attributed to P-selectin-mediated cancer cell targeting. Next, we investigated the therapeutic potential of DTSPs-3 and DTSLs in synergy with HIFU ablation. In this step, HeLa cells incubated with drug-loaded vesicles were exposed to HIFU hyperthermia (42 °C for 2 min) for triggered drug release, followed by treatment with HIFU ablation for 30 s, and then the cells were cultured for 24 h at 37 °C. Our results showed that HIFU ablation improved the outcome of HIFU hyperthermia-triggered chemotherapy in the growth inhibition of cancer cells (Figure 4E). Interestingly, under the same HIFU treatment conditions, HeLa cells treated with DTSPs-3 exhibited lower cell viability than cells treated with DTSLs, indicating the high chemotherapeutic efficiency of DTSPs-3 in combination with HIFU ablation.

### **In vivo blood circulation and biodistribution of TSPs-3.**

The *in vivo* blood circulation profile and biodistribution of TSPs-3 were investigated in

comparison with TSLs and DMLs. All vesicles were incorporated with TopFluor® PC and were intravenously injected into mice bearing transplanted HeLa cell tumors. The blood retention curves and biodistribution of the vesicles were evaluated by detection of the TopFluor® PC content. As shown in Figure 5A, the blood circulation profile of TSPs-3 was comparable to that of TSLs but significantly prolonged compared to that of DMLs. At 24 h after injection, TSPs-3 exhibited a blood retention of 16.3% ID/g, which was slightly lower than that of TSLs (18.9% ID/g) but much higher than that of DMLs (2.4% ID/g). Then, we compared the biodistribution of different vesicles in the tumors and major organs of mice at different time points following injection. As shown in Figure 5B-D, all vesicles were mainly accumulated in the liver, spleen and lungs at 24 h postinjection. Among the vesicles, DMLs undergo fast clearance by the liver, spleen and lungs but do not effectively accumulate in the tumor. In contrast, TSPs-3 and TSLs had relatively slower accumulations in the organs but showed gradually increased accumulations in the tumor. Notably, TSPs-3 exhibited nearly 2.5-, 2.0- and 2.8-fold greater accumulation than TSLs at 4, 12 and 24 h postinjection, respectively. Our findings showed that the incorporation of the PM not only obtained benefits comparable to those of a conventional pegylation strategy in improving the blood circulation of liposomal vesicles but also significantly enhanced the tumor targeting efficacy of liposomal vesicles. The improved pharmacokinetic behavior and tumor targeting efficacy of TSPs-3 can be attributed to the

immune evasion potential of the PM [20,27] and P-selectin-mediated active tumor targeting.

### Vascular damage and inflammation response of TSPs-3 post HIFU ablation.

Gu and colleagues reported that artificially triggered tumor vascular inflammation can improve the tumor targeting efficiency of PM-coated nanoparticles due to their PLT-like adhesion to injured vasculature [26]. Theoretically, HIFU beams not only ablate cancer cells but also destroy the tumor vasculature. Therefore, HIFU-induced tumor vascular damage and inflammation may make PM-incorporated TSPs easy to target the postoperative tumor site. We first evaluated HIFU-induced inflammation and vascular damage at the postoperative tumor site. The production of inflammatory cytokines, including TNF- $\alpha$ , IL-6 and IL-8, significantly increased after HIFU ablation (Figure 6A-C). The tumor vasculature after HIFU ablation showed the increased expression of the inflammatory biomarker VCAM-1 compared with the untreated group (Figure 6D). Additionally, hematology analysis showed that the levels of white blood cells (WBCs) and PLTs were elevated after HIFU ablation (Figure S7). These results indicated that HIFU ablation triggered severe inflammation and vascular damage in the postoperative tumor site. To demonstrate that TSPs-3 can selectively accumulate in the postoperative tumor sites through HIFU-induced tumor vascular damage and inflammation, HeLa cell tumor-bearing mice were treated with HIFU ablation followed by the administration of TSPs-3 at 6 h after

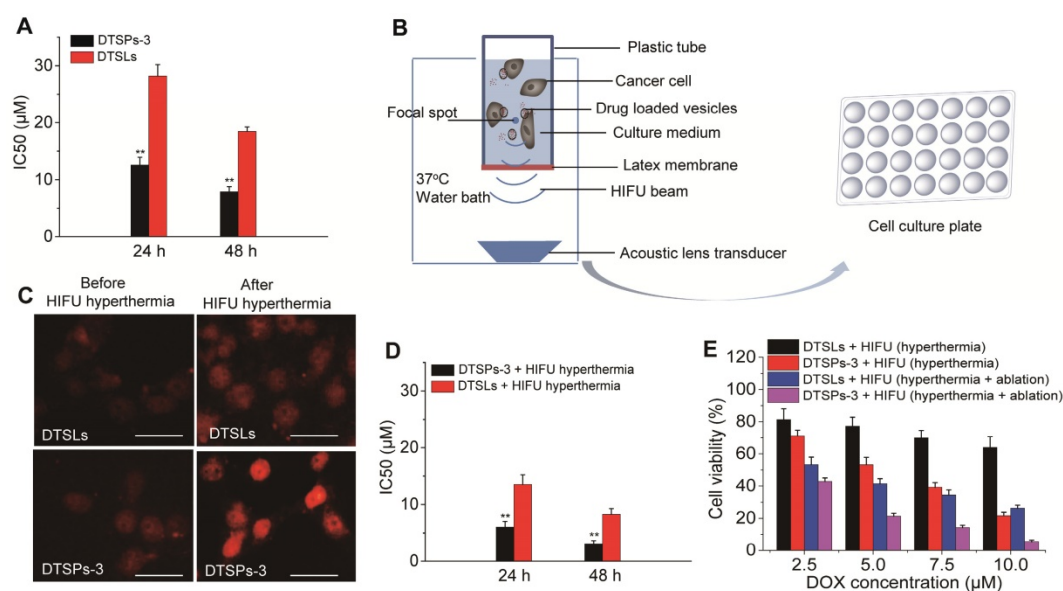


**Figure 4.** (A) IC50 values of DTSPs-3 and DTSLs against HeLa cells. (B) Schematic illustration of the design and apparatus for evaluation of the therapeutic potential of drug-loaded vesicles in combination with HIFU hyperthermia and ablation. (C) Fluorescence signals of DOX in HeLa cells incubated with drug-loaded vesicles before and after HIFU hyperthermia. The scale bar represents 20  $\mu$ m. (D) IC50 values of HeLa cells after treatment with DTSPs-3 and DTSLs in combination with HIFU hyperthermia. (E) Viability of HeLa cells after different treatments.

HIFU ablation. Mice treated with TSPs-3 alone or HIFU ablation + TSPs-3 were used for comparison. For *in vivo* tracking, the vesicles were incorporated with TopFluor® PC. As observed in Figure 6E, TSPs-3 rapidly accumulated at the tumor site of mice pretreated with HIFU irradiation, and nearly 45% ID/g was detected in tumor tissue at 2 h postinjection (Figure 6F). This phenomenon was not observed in the two control groups. This result indicated that HIFU-induced tumor vascular damage and inflammation triggered the ultrafast and accurate accumulation of TSPs-3 to the postoperative tumor site. Therefore, we believe that the prompt response of TSPs-3 to vascular damage and inflammation is advantageous for implementing ideal postoperative consolidation chemotherapy after HIFU ablation.

### Therapeutic performance of DTSPs-3 in combination with HIFU ablation.

The therapeutic performance of DTSPs-3 in combination with HIFU ablation was investigated in the HeLa cell tumor-bearing mouse model and was compared with the performance of free DOX and DTSLs. To implement synergistic HIFU chemotherapy, we treated the tumors with HIFU hyperthermia (42 °C) for 20 min and closely followed HIFU ablation for 30 s after drug injection (Figure 7A). HIFU hyperthermia was used to improve tumor drug availability before HIFU ablation. The tumor drug delivery efficiency of DTSPs-3 and DTSLs upon HIFU hyperthermia was investigated. TopFluor® PC was used to label DTSPs-3 and DTSLs to quantify their tumor uptake. For mice treated with DTSPs-3 and DTSLs, the DOX and TopFluor® PC contents in tumor

tissue were significantly enhanced upon HIFU hyperthermia (Figure 7B,C). Additionally, the measured DOX content in the treated tumor tissue was much greater than the theoretical DOX content (in direct proportion to the TopFluor® PC content), as shown in Figure 7C. These results indicated that HIFU hyperthermia not only increased the tumor uptake of vesicles but also triggered the rapid release of DOX from vesicles in the tumor vasculature to enhance tumor drug availability. Under HIFU hyperthermia, the tumor uptake of DTSPs-3 was approximately 1.9-fold greater than that of DTSLs, and the drug availability of DTSPs-3-treated tumors was nearly 2-fold and 10-fold greater than that of DTSLs and free DOX groups, respectively, demonstrating the high tumor affinity and temperature-sensitive drug delivery efficacy of TSPs-3. Notably, a sudden increase in tumor drug availability (nearly 37.5% ID/g) was observed in the DTSPs-3 + HIFU group at 4-10 h after HIFU ablation (Figure 7D). By immunofluorescent observation, we found that DTSPs-3 was distributed more widely than DTSLs and free DOX in the tumor tissue after HIFU ablation, and the red fluorescent from DOX merged well with the green fluorescent from VCAM-1 antibody on inflammatory tumor vasculature (Figure 7E). It proved that DTSPs-3 could efficiently target the inflammatory tumor vasculature after HIFU ablation by a PLT-like property. The above results demonstrated that DTSPs-3 could improve drug availability at the tumor site before and after HIFU ablation.

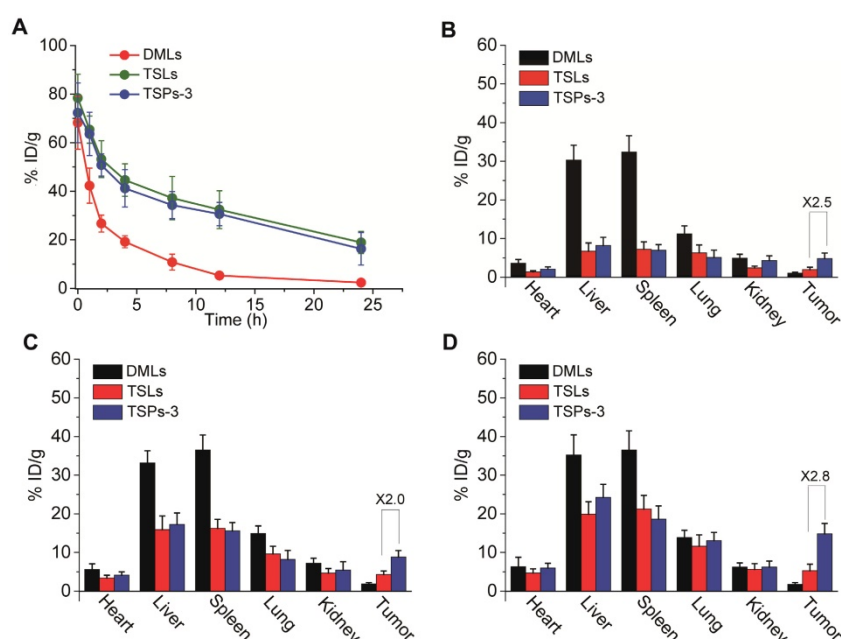


**Figure 5.** (A) Blood retention curves of DMLs, TSLs and TSPs-3 in mice over a span of 24 h after intravenous injection. (B-D) Biodistribution of DMLs, TSLs and TSPs-3 in mice at 4, 12 and 24 h after intravenous injection.

The tumor growth of different treatment groups is shown in Figure 8A. Within 18 days after treatment, the tumor volume in the saline group increased to approximately 1223 mm<sup>3</sup>. In the HIFU-alone treatment group, the tumor temperature was elevated from 42 °C to approximately 68.7 °C within 30 s of HIFU ablation and remained above 48 °C for another 270 s (Figure 8B). The ablation treatment could inhibit tumor growth in the treated mice. Compared with HIFU-alone treatment, the synergistic therapies, which employed free DOX, DTSLs and DTSPs-3 in combination with HIFU treatment, demonstrated diverse therapeutic outcomes. Among synergistic therapies, free DOX exhibited minimal chemotherapeutic efficiency in combination with HIFU treatment for tumor inhibition due to the lowest tumor drug availability. In the DTSLs + HIFU treatment group, the tumor volume increased to approximately 329 mm<sup>3</sup>. In stark contrast, the tumor volume in the DTSPs-3 + HIFU treatment group

decreased to 35 mm<sup>3</sup>. By H&E and TUNEL staining, the increased death of tumor cells was observed in the DTSPs-3 + HIFU treatment group compared with that in the other treatment groups (Figure 8C) at 24 h after HIFU treatment. Therefore, our results indicated that TSPs-3 can act as a more efficient chemotherapy platform in combination with HIFU treatment for tumor therapy. No apparent changes were found in the histology of the main organs (liver, heart, spleen, lungs and kidney) and hematology in the DTSPs-3 + HIFU treatment group compared with those in the saline and DTSLs + HIFU treatment groups at the conclusion of the *in vivo* antitumor study (Figure S8 and Table S2), suggesting the safety of TSPs-3 for *in vivo* medical applications. Notably, however, PLT proteins are immunogenic constructs [35]. Thus, many issues associated with the intracorporal influence of PLT-based nanomedicine, especially *in vivo* immunotoxicity, will be fully investigated by us in follow-up studies.

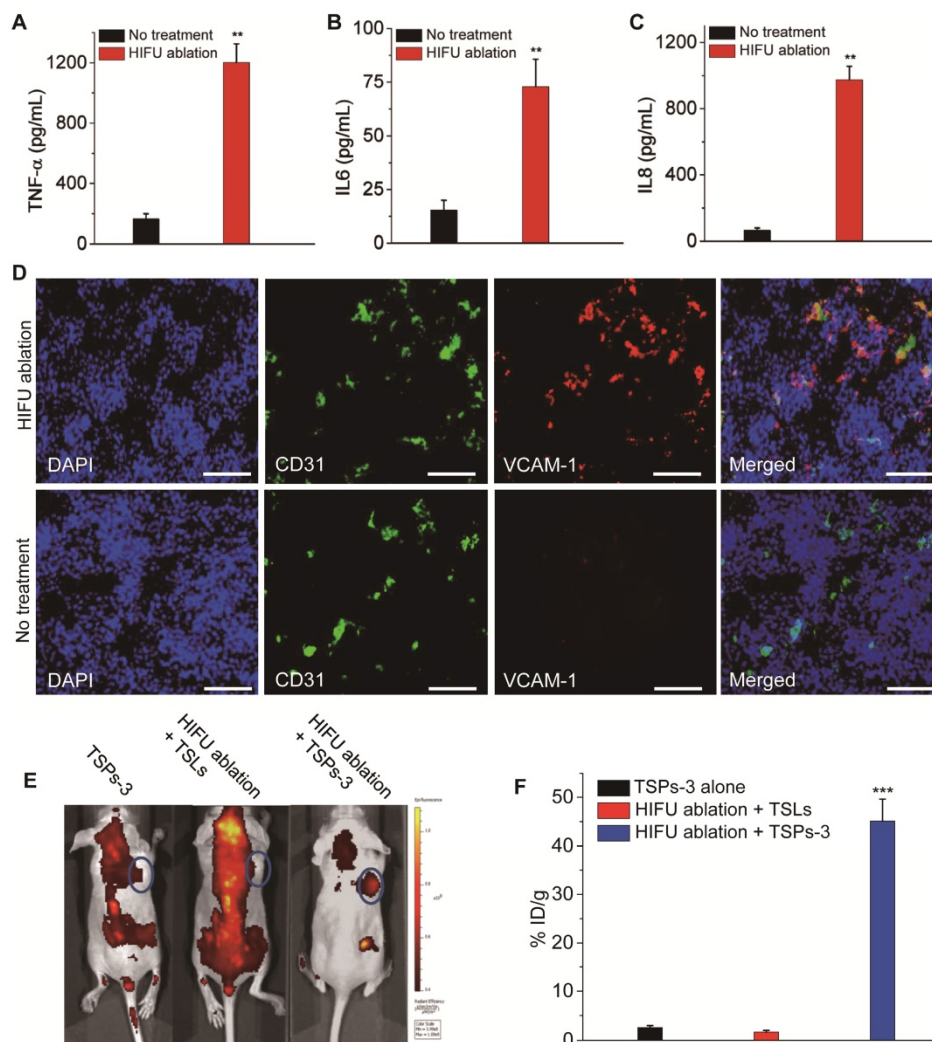


**Figure 6.** Increase in (A) TNF- $\alpha$ , (B) IL-6 and (C) IL-8 in the blood samples of mice at 6 h after HIFU tumor ablation. (D) Increased expression of VCAM-1 in tumor vasculature at 6 h after HIFU tumor ablation (red signal, VCAM-1; blue signal, cell nucleus; green signal, CD31). The scale bar represents 200  $\mu$ m. (E) Fluorescence images of HeLa cell tumor-bearing mice at 2 h after intravenous injection of different vesicles when the tumors were pretreated with HIFU ablation. (F) Targeting efficiency of different vesicles to HeLa cell tumors pretreated with or without HIFU ablation.

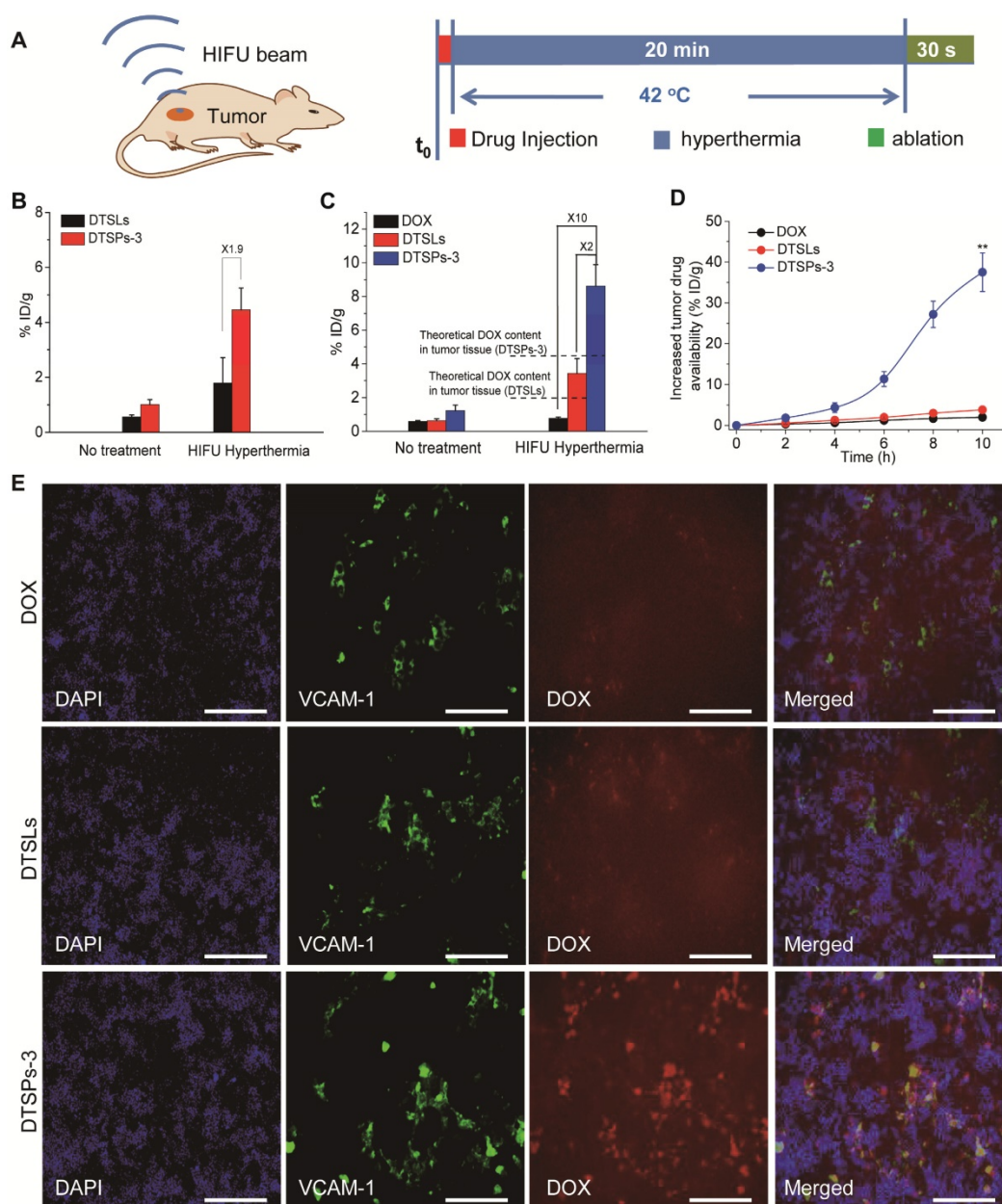


**Figure 7.** (A) Schematic design used to investigate synergistic HIFU chemotherapy. (B) Tumor uptake of DTSLs and DTSPs-3 with or without HIFU hyperthermia. (C) Tumor drug availability after the administration of free DOX, DTSLs and DTSPs-3 with or without HIFU hyperthermia. (D) The increase in tumor drug availability in the free DOX, DTSLs and DTSPs-3 groups at 10 h after HIFU ablation (red signal, DOX; blue signal, DAPI; green signal, VCAM-1). The scale bar represents 200 μm.

## Conclusions

TSPs, as PLT-mimicking liposomal nanovesicles, were successfully constructed by integrating DPPC, MSPC, and PM. TSPs displayed high drug loading efficiency, temperature-sensitive permeability, improved blood circulation and PLT-like properties, such as cancer cell affinity and the vascular damage response, in a mouse model. Compared with TSLs, TSPs demonstrated enhanced tumor uptake and provided increased tumor drug availability upon HIFU hyperthermia in mice, providing efficient chemotherapy in combination with HIFU ablation.

Similar to PLT activities, TSPs spontaneously targeted the postoperative tumor site by adhesion to the damaged tumor vasculature after HIFU ablation, leading to ideal consolidation chemotherapy. Thus, TSPs could be an impressive achievement of smart nanoparticle design to cooperate with HIFU in cancer therapy. Additionally, there are still many issues that need to be systematically investigated and addressed in the future, especially the immunotoxicity of TSPs and how to make the TSPs-mediated drug delivery approach feasible in the human body, which has a high circulation volume and a more complex physiological environment.

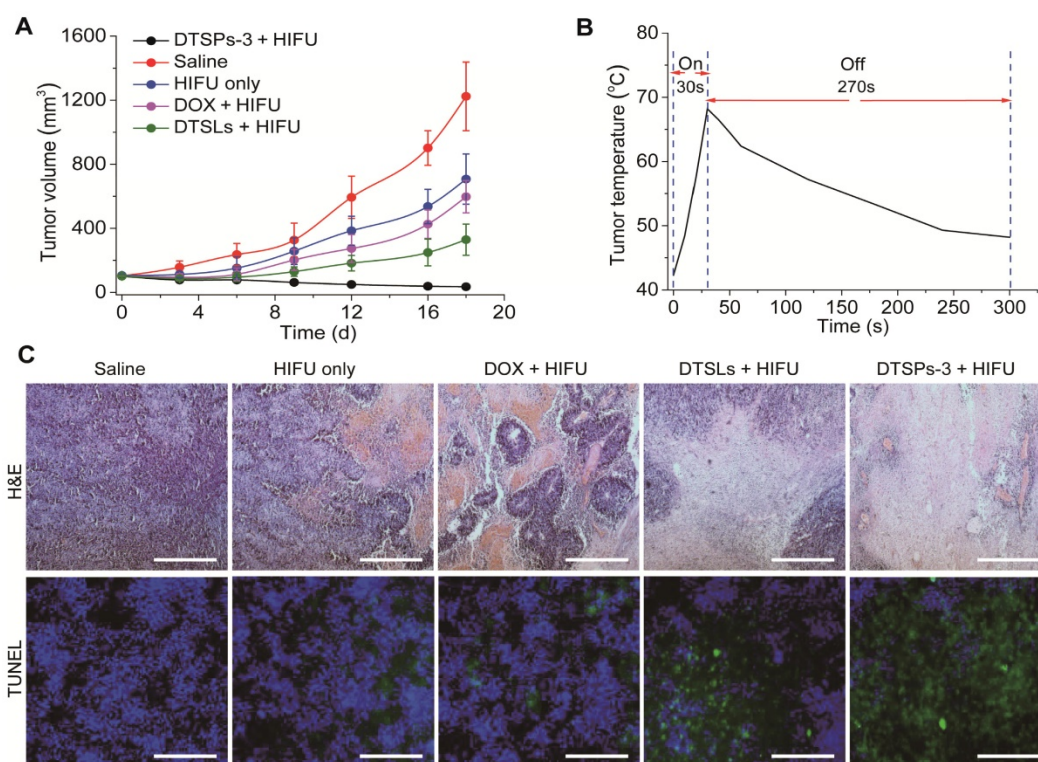


**Figure 8.** (A) Tumor growth curves of different treatment groups. (B) Temperature elevation at the tumor site after 30 s of HIFU ablation from an initial temperature of 42 °C. (C) H&E staining and TUNEL assay of the tumor tissues at 24 h after different treatments (Scale bar = 200 μm).

## Abbreviations

HIFU: high-intensity focused ultrasound; NDDSs: nanosized drug delivery systems; MSPC: 1-stearoyl-2-hydroxy-sn-glycero-3-phosphocholine; DPPC: 1,2-dipalmitoyl-sn-glycero-3-phosphocholine; PEG: poly(ethylene glycol); TopFluor®PC: 1-palmitoyl-2-(dipyrometheneborondifluoride)undecanoyl-sn-glycero-3-phosphoethanolamine; TopFluor® Lyso PC: 1-(dipyrometheneboron difluoride)undecanoyl-2-hydroxy-sn-glycero-3-phosphocholine; DSPE-PEG<sub>2000</sub>: 1,2-distearoyl-sn-glycero-3-phosphoethanolamine-N-[methoxy(polyethylene glycol)-2000]; PLT: platelet; PM: platelet membrane; TSPs: temperature-sensitive plateletsomes; NPVs: nanoscale platelet vesicles; TSLs: temperature-sensitive liposomes; DMLs: liposomes made from DPPC and MSPC; DOX: doxorubicin; DiR iodide: 1,1'-dioctadecyl-3,3',3'-tetramethylindotricarbocyanine iodide; MTT: methylthiazolyldiphenyl-tetrazolium bromide; TEM: transmission electron microscopy; Tm: phase transition temperature; PBS: phosphate buffered solution.

## Supplementary Material

Supplementary figures and tables.

<http://www.thno.org/v09p3966s1.pdf>

## Acknowledgements

Dongqi Wu, Xing Jin and Xiaobing Wang contributed equally to this work. This work was financially supported by National Natural Science Foundation of China (No. 81701822), Heilongjiang Province Science Foundation for Youths (No. QC2018090), China Postdoctoral Science Foundation (No. 2016M600238), Heilongjiang Postdoctoral Special Fund (No. LBH-TZ1601), Northeast Forestry University Double First-Rate Construction Fund (No.000/41113281) and the Fundamental Research Funds for Central Universities (No. 2572017PZ09).

## Competing Interests

The authors have declared that no competing interest exists.

## References

- Kennedy JE. High-intensity focused ultrasound in the treatment of solid tumours. *Nat Rev Cancer*. 2005; 5(4): 321-7.
- Kennedy JE, ter Haar GR, Cranston D. High intensity focused ultrasound: surgery of the future? *Br J Radiol*. 2003; 76 (909): 590-9.
- Tempany CM, McDannold NJ, Hynynen K, Jolesz FA. Focused ultrasound surgery in oncology: overview and principles. *Radiology* 2011; 259(1): 39-56.
- Schmitz AC, Gianfelice D, Daniel BL, Mali WP, van den Bosch MA. Image-guided focused ultrasound ablation of breast cancer: current status, challenges, and future directions. *Eur Radiol*. 2008;18(7):1431-41.
- Bailey MR, Khokhlova VA, Sapozhnikov OA, Kargl SG, Crum LA. Physical mechanisms of the therapeutic effect of ultrasound - a review. *Acoust Phys*. 2003; 49: 369-88.
- Ma M, Xu H, Chen H, Jia X, Zhang K, Wang Q, et al. A drug-perfluorocarbon nanoemulsion with an ultrathin silica coating for the synergistic effect of

- chemotherapy and ablation by high-intensity focused ultrasound. *Adv Mater.* 2014; 26(43): 7378-85.
7. Wang X, Chen H, Chen Y, Ma M, Zhang K, Li F, et al. Perfluorohexane-encapsulated mesoporous silica nanocapsules as enhancement agents for highly efficient high intensity focused ultrasound (HIFU). *Adv Mater.* 2012; 24(6): 785-91.
  8. Chen Y, Chen H, Sun Y, Zheng Y, Zeng D, Li F, et al. Multifunctional mesoporous composite nanocapsules for highly efficient MRI-guided high-intensity focused ultrasound cancer surgery. *Angew Chem Int Ed Engl.* 2011; 50(52): 12505-9.
  9. Park EJ, Ahn YD, Lee JY. In vivo study of enhanced chemotherapy combined with ultrasound image-guided focused ultrasound (USgFUS) treatment for pancreatic cancer in a xenograft mouse model. *Eur Radiol.* 2018; 28(9): 3710-8.
  10. Poff JA, Allen CT, Traughber B, Colunga A, Xie J, Chen Z, et al. Pulsed high-intensity focused ultrasound enhances apoptosis and growth inhibition of squamous cell carcinoma xenografts with proteasome inhibitor bortezomib. *Radiology.* 2008; 248: 485-91.
  11. Tang H, Guo Y, Peng L, Fang H, Wang Z, Zheng Y, et al. In vivo targeted, responsive, and synergistic cancer nanotheranostics by magnetic resonance imaging-guided synergistic high-intensity focused ultrasound ablation and chemotherapy. *ACS Appl Mater Interfaces.* 2018; 10(18): 15428-41.
  12. Arora JS, Murad HY, Ashe S, Halliburton G, Yu H, He J, et al. Ablative focused ultrasound synergistically enhances thermally triggered chemotherapy for prostate cancer in vitro. *Mol Pharm.* 2016; 13(9): 3080-90.
  13. Hijnen N, Kneepkens E, de Smet M, Langereis S, Heijman E, Grüll H. Thermal combination therapies for local drug delivery by magnetic resonance-guided high-intensity focused ultrasound. *Proc Natl Acad Sci U S A.* 2017; 114(24): E4802-11.
  14. Li SD, Huang L. Stealth nanoparticles: high density but sheddable PEG is a key for tumor targeting. *J Control Release.* 2010; 145(3): 178-81.
  15. Maldiney T, Richard C, Seguin J, Wattier N, Bessodes M, Scherman D. Effect of core diameter, surface coating, and PEG chain length on the biodistribution of persistent luminescence nanoparticles in mice. *ACS Nano.* 2011; 5(2): 854-62.
  16. Wu F, Chen WZ, Bai J, Zou JZ, Wang ZL, Zhu H, et al. Tumor vessel destruction resulting from high-intensity focused ultrasound in patients with solid malignancies. *Ultrasound Med Biol.* 2002; 28(4): 535-42.
  17. Vaezy S, Zderic V. Hemorrhage control using high intensity focused ultrasound. *Int J Hyperthermia.* 2007; 23(2): 203-11.
  18. Hu CM, Fang RH, Wang KC, Luk BT, Thamphiwatana S, Dehaini D, et al. Nanoparticle biointerfacing by platelet membrane cloaking. *Nature.* 2015; 526: 118-21.
  19. Hu Q, Qian C, Sun W, Wang J, Chen Z, Bomba HN, et al. Engineered nanoplatelets for enhanced treatment of multiple myeloma and thrombus. *Adv Mater.* 2016; 28(43): 9573-80.
  20. Rao L, Bu LL, Meng QF, Cai B, Deng WW, Li A, et al. Antitumor platelet-mimicking magnetic nanoparticles. *Adv Funct Mater.* 2017; 27: 1604774.
  21. Dehaini D, Wei X, Fang RH, Masson S, Angsantikul P, Luk BT, et al. Erythrocyte-platelet hybrid membrane coating for enhanced nanoparticle functionalization. *Adv Mater.* 2017; 29(16): 1606209.
  22. Rao L, Meng Q, Huang Q, Wang Z, Yu G, Li A, et al. Platelet-leukocyte hybrid membrane-coated immunomagnetic beads for highly efficient and highly specific isolation of circulating tumor cells. *Adv Funct Mater.* 2018; 28: 1803531.
  23. Rao L, Bu LL, Ma L, Wang W, Liu H, Wan D, et al. Platelet-facilitated photothermal therapy of head and neck squamous cell carcinoma. *Angew Chem Int Ed Engl.* 2018; 57(4): 986-91.
  24. Hu Q, Sun W, Qian C, Wang C, Bomba HN, Gu Z. Anticancer platelet-mimicking nanovehicles. *Adv Mater.* 2015; 27: 7043-50.
  25. Wang C, Sun WJ, Ye YQ, Hu QY, Bomba HN, Gu Z. In situ activation of platelets with checkpoint inhibitors for post-surgical cancer immunotherapy. *Nat Biomed Eng.* 2017; 1: 0011.
  26. Hu Q, Sun W, Qian C, Bomba HN, Xin H, Gu Z. Relay drug delivery for amplifying targeting signal and enhancing anticancer efficacy. *Adv Mater.* 2017; 29: 1605803.
  27. Jing L, Qu H, Wu D, Zhu C, Yang Y, Jin X, et al. Platelet-camouflaged nanococktail: simultaneous inhibition of drug-resistant tumor growth and metastasis via a cancer cells and tumor vasculature dual-targeting strategy. *Theranostics.* 2018; 8(10): 2683-95.
  28. Xu L, Gao F, Fan F, Yang L. Platelet membrane coating coupled with solar irradiation endows a photodynamic nanosystem with both improved antitumor efficacy and undetectable skin damage. *Biomaterials.* 2018; 159: 59-67.
  29. Landon CD, Park JY, Needham D, Dewhirst MW. Nanoscale drug delivery and hyperthermia: the materials design and preclinical and clinical testing of low temperature-sensitive liposomes used in combination with mild hyperthermia in the treatment of local cancer. *Open Nanomed J.* 2011; 3: 38-64.
  30. Henle KJ, Dethlefsen LA. Heat fractionation and thermotolerance: a review. *Cancer Res.* 1978; 38(7): 1843-51.
  31. Jaque D, Martínez Maestro L, del Rosal B, Haro-Gonzalez P, Benayas A, Plaza JL, et al. Nanoparticles for photothermal therapies. *Nanoscale.* 2014; 6(16): 9494-530.
  32. Thüroff S, Chaussy C, Vallancien G, Wieland W, Kiel HJ, Le Duc A, et al. High-intensity focused ultrasound and localized prostate cancer: efficacy results from the European multicentric study. *J Endourol.* 2003; 17(8): 673-7.
  33. Crouzet S, Murat FJ, Pasticier G, Cassier P, Chapelon JY, Gelet A. High intensity focused ultrasound (HIFU) for prostate cancer: current clinical status, outcomes and future perspectives. *Int J Hyperthermia.* 2010; 26(8): 796-803.
  34. Liang X, Gao J, Jiang L, Luo J, Jing L, Li X, et al. Nanohybrid liposomal cerasomes with good physiological stability and rapid temperature responsiveness for high intensity focused ultrasound triggered local chemotherapy of cancer. *ACS Nano.* 2015; 9(2): 1280-93.
  35. Landau M, Rosenberg N. Molecular insight into human platelet antigens: structural and evolutionary conservation analyses offer new perspective to immunogenic disorders. *Transfusion.* 2011; 51(3): 558-69.